Regionality of deep low-frequency earthquakes associated with subduction of the Philippine Sea plate along the Nankai Trough, southwest Japan

Shoichi Yoshioka [a,*], Mamiko Toda [b], Junichi Nakajima [c]

[a] Department of Earth and Planetary Sciences, Faculty of Sciences, Kyushu University, Hakozaki 6-10-1, Higashi ward, Fukuoka 812-8581, Japan
[b] Mitsubishi Space Software Co., Ltd, 32nd floor, World Trade Center building, Hamamatsu-cho, Minato ward, Tokyo 105-0013, Japan
[c] Research Center for Prediction of Earthquakes and Volcanic Eruptions, Graduate School of Science, Tohoku University, Aoba, Aramaki-aza, Aoba ward, Sendai 980-8578, Japan

ARTICLE INFO

ABSTRACT

The Fukuoka District Meteorological Observatory recently logged three possible deep low-frequency earthquakes (LFEs) beneath eastern Kyushu, Japan, a region in which LFEs and low-frequency tremors have never before been identified. To assess these data, we analyzed band-pass filtered velocity seismograms and relocated LFEs and regular earthquakes using the double-difference method. The results strongly suggest that the three events were authentic LFEs, each at a depth of about 50 km. We also performed relocation analysis on LFEs recorded beneath the Kii Peninsula and found that these LFEs occurred near the northwest-dipping plate interface at depths of approximately 29–38 km. These results indicate that LFEs in southwest Japan occur near the upper surface of the subducting Philippine Sea (PHS) plate. To investigate the origin of regional differences in the occurrence frequency of LFEs in western Shikoku, the Kii Peninsula, and eastern Kyushu, we calculated temperature distributions associated with PHS plate subduction. Then, using the calculated thermal structures and a phase diagram of water dehydration for oceanic basalt, the water dehydration rate (wt.%/km), which was newly defined in this study, was determined to be 0.19, 0.12, and 0.08 in western Shikoku, the Kii Peninsula, and eastern Kyushu, respectively; that is, the region beneath eastern Kyushu has the lowest water dehydration rate value. Considering that the Kyushu–Palau Ridge that is subducting beneath eastern Kyushu is composed of tonalite, which is low in hydrous minerals, this finding suggests that the regionality may be related to the amount of water dehydration associated with subduction of the PHS plate and/or differences in LFE depths. Notable dehydration reactions take place beneath western Shikoku and the Kii Peninsula, where the depth ranges for dehydration estimated by thermal modeling agree well with those for the relocated LFEs. The temperature range in which LFEs occur in these regions is estimated to be 400–500 °C.

© 2008 Elsevier B.V. All rights reserved.

1. Introduction

The Nankai Trough is a convergent plate boundary where the oceanic Philippine Sea (PHS) plate is subducting beneath the continental Amuria (AM) plate northwestward in southwest Japan (Fig. 1). Large M8-class interplate earthquakes have occurred repeatedly off Shikoku and the Kii Peninsula at intervals of approximately 90 to 150 years (e.g., Ando, 1975).

Since October 1997, short-period seismograms recorded at seismic stations throughout Japan installed and maintained by universities, the National Research Institute for Earth Science and Disaster Prevention (NIED), the Japan Meteorological Agency (JMA), national institutes, and local governments have been transmitted to the JMA. The JMA has processed the data collected to date to create a comprehensive seismic catalogue for Japan. Data from Hi-net stations, a dense network of highly sensitive short-period instruments installed by the NIED, have been included in the database since October 2000 and have remarkably improved detection ability. One of the advantages of the JMA catalogue is that it provides almost the same detectability beneath all of the Japanese Islands, due to a densely deployed nationwide seismograph network with a station separation of ~20 km.

This enhanced and uniform detectability has led to the discovery of deep low-frequency earthquakes (LFEs) and low-frequency tremors (LFTs) accompanied by aseismic slow slip events in the downdip extensions of the Nankai subduction zone (e.g., Obara, 2002; Katsumata and Kamaya, 2003; Obara and Hirose, 2006). LFEs are identified from S waves detected during LFTs.

LFTs beneath Shikoku and the Kii Peninsula are characterized by long duration and source mobility. LFTs last for several days to a couple of weeks (Obara, 2002). Tremor sources tend to move in the northeast or southwest direction along the isodepth contours of the upper surface of the subducted PHS plate (Obara and Hirose, 2006). The epicenters of LFTs and LFEs are distributed along the isodepth contours in a belt-like form (Fig. 1). Based on these characteristics, LFT generation is considered to be related to dehydration associated with subduction of the PHS plate (Obara, 2002). LFEs and LFTs have not been identified in northeast Japan, the Kanto district, Kii channel, and Kyushu.

* Corresponding author. Tel.: +81 92 642 2646; fax: +81 92 642 2684.
E-mail address: yoshioka@geo.kyushu-u.ac.jp (S. Yoshioka).
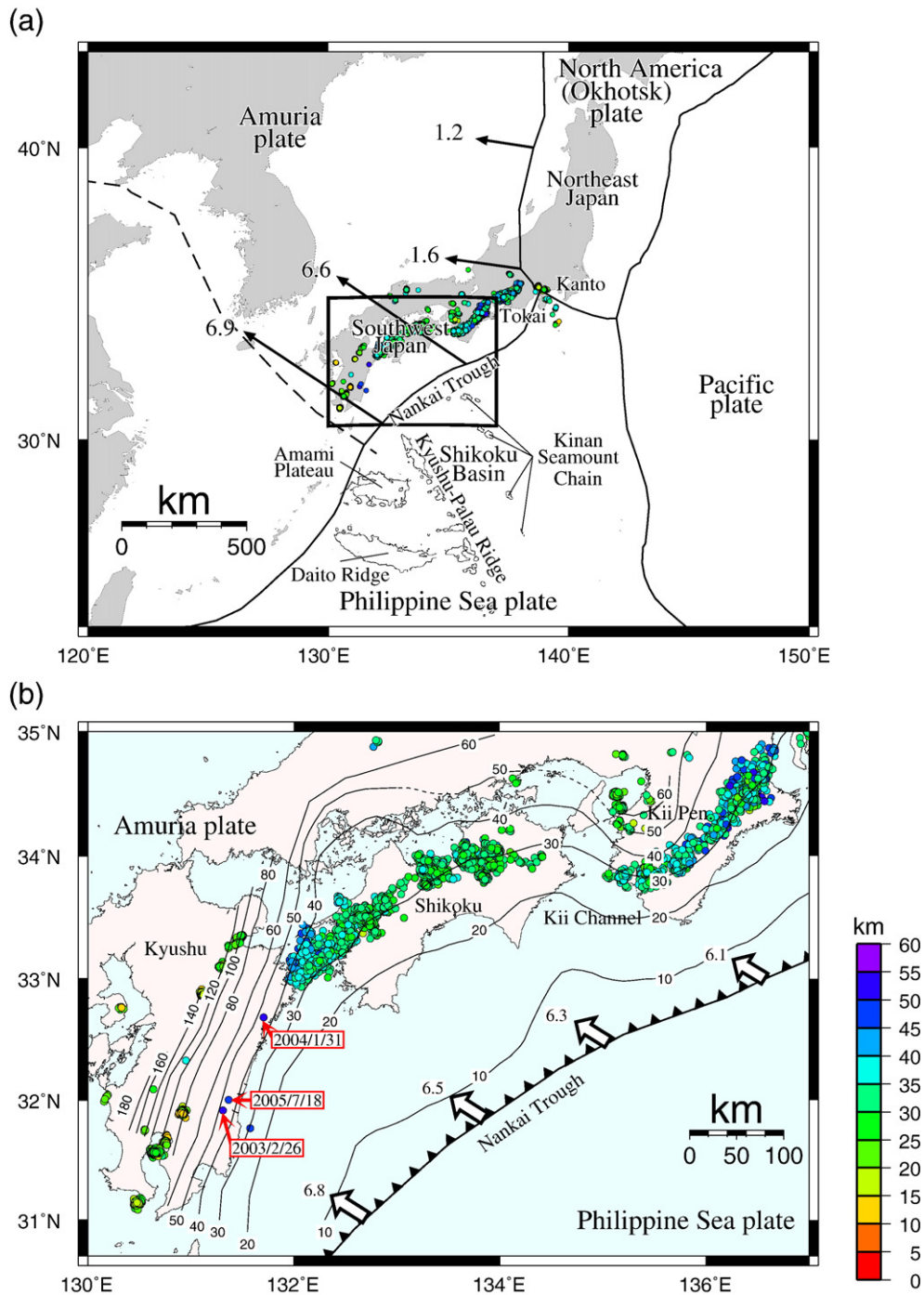
Fig. 1. (a) Tectonic map in and around the Japanese Islands. Plate motion velocity vectors (cm/yr) of the Amuria (AM) plate relative to the adjacent plates are shown in numerals (Wei and Seno, 1998). Epicenters of low-frequency earthquakes (LFEs) determined by the Japan Meteorological Agency (JMA) are shown with color solid circles. Colors of the circles denote hypocenter depths reported in the JMA hypocenter catalogue. The dashed line is the plate boundary where the location is not clear. The Amami Plateau and the Daito Ridge, the Kyushu–Palau Ridge, and the Kinan Seamount Chain are delineated by isodepth contours of 4000, 3000, and 3500 m, respectively. (b) Detailed tectonic map in the boxed region shown in (a). Epicenters of low-frequency earthquakes (LFEs) determined by the JMA are shown with color solid circles. Colors of the circles denote hypocenter depths reported in the JMA hypocenter catalogue. Locations of the three possible LFEs that occurred beneath eastern Kyushu are shown with the arrows with the dates of their occurrences. The solid curved lines are isodepth contours of the upper surface of the subducting Philippine Sea (PHS) plate along the Nankai Trough estimated from the results by Baba et al. (2002), Nakajima and Hasegawa (2007), and Hirose et al. (2007). The open arrows with numerals along the Nankai Trough are plate motion vectors (cm/yr) of the PHS plate with respect to the AM plate (Sella et al., 2002).

However, four possible LFEs were recorded beneath eastern Kyushu at depths of about 50 km (e.g., Fukuoka District Meteorological Observatory, 2004a). While listed in the JMA hypocenter catalogue, because of the qualitative definition of LFEs used by the JMA and the rarity of events beneath eastern Kyushu, the authenticity of these records is controversial. Therefore, we assessed these data quantitatively using band-pass filtered seismic waveforms and relocation analysis (hypo-center estimation relative to regular intraslab microearthquakes) using a double-difference (DD) location technique. Determining a precise location relative to regular intraslab earthquakes is very important in quantitative interpretation of LFE occurrence.

In addition, we discuss the regionality of LFEs beneath western Shikoku, the Kii Peninsula, and eastern Kyushu, based on 2-D numerical simulations of temperature structures associated with subduction

of the PHS plate and the dehydration process of oceanic basalt. Temperature fields and pressure and temperature conditions of hydrous minerals in the oceanic crust associated with PHS plate subduction have already been estimated for southwest Japan (e.g., Wang et al., 1995; Hyndman et al., 1995; Oleskevich et al., 1999; Peacock and Wang, 1999; Hacker et al., 2003b). The differences between these previous studies and our model are also discussed.

2. Data analyses

2.1. LFE distribution in southwest Japan

The LFEs were recorded beneath Shikoku and the Kii Peninsula in belt-like forms along the isodepth contours of the subducted PHS plate (Fig. 1(b)). The JMA database identifies deep non-volcanic LFEs based on the following mostly qualitative criteria: 1) Most LFEs are microearthquakes of M 2.0 or less; 2) LFEs have seismic waveforms with a dominant low-frequency component, their occurrence as a single event is rare, and in general several earthquakes occur successively; 3) In general, although it is difficult to identify the onset of the P wave, the onset of the S wave can often be determined, and usually their hypocenter depths are 20–30 km (Yamada, personal communication).

The JMA hypocenter catalogue includes four possible LFE hypocenters located beneath eastern Kyushu (Fukuoka District Meteorological Observatory, 2004a) for the period of October 1997 – January 2007. However, one of the four possible LFEs off the east coast of Kyushu was misidentified and was actually a very low-frequency earthquake that occurred in the accretionary prism on the continental slope of the Nankai Trough (Fukuoka District Meteorological Observatory, 2004b; Ito and Obara, 2006). The other three possible LFEs occurred at depths of about 50 km, which is close to the isodepth contours of the upper surface of the PHS plate (Fig. 1(b)). Incidentally, LFEs located in central and western regions of Kyushu in Fig. 1(b) originated from shallow volcanic activity. Unlike LFEs beneath Shikoku and the Kii Peninsula, which occurred during continuous LFTs, the possible LFEs beneath eastern Kyushu were isolated events (Obara, personal communication).

2.2. Band-pass filtered analysis of seismic velocity waveforms

To assess whether the three possible LFEs were authentic low-frequency events, we performed band-pass filtered analysis of velocity seismograms. Fig. 2(a)–(c) show the north–south (NS) components of the band-pass filtered seismic velocity waveforms at stations with epicentral distances of about 30 km for the three possible LFEs, which
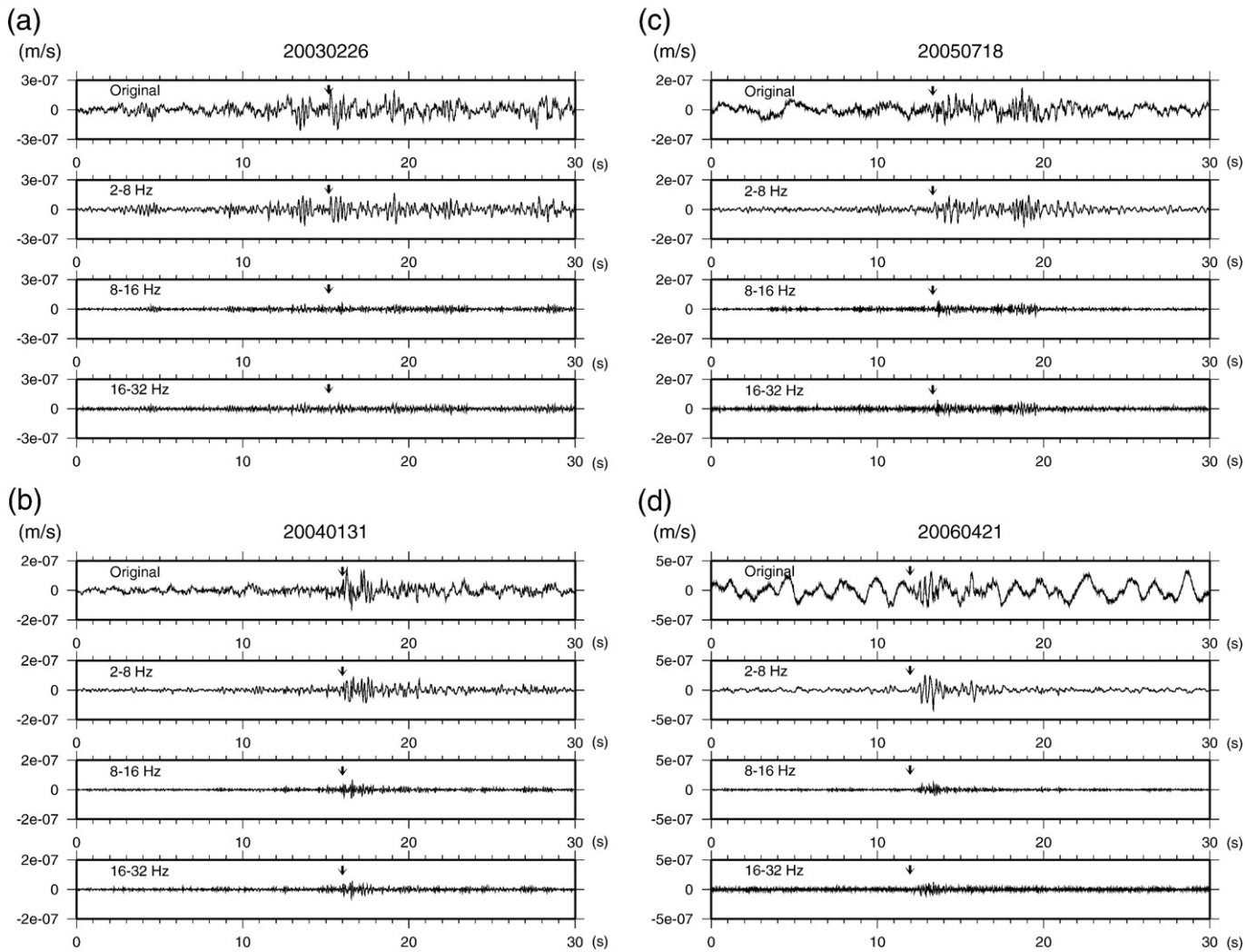
Fig. 2. The NS components of original and band-pass filtered (2–8, 8–16, 16–32 Hz) velocity seismic waveforms for the possible LFEs that occurred at depths of about 50 km beneath eastern Kyushu ((a), (b), and (c)) and an LFE that occurred at a depth of about 30 km beneath western Shikoku ((d)) recorded at stations with an epicentral distance of about 30 km (from top to bottom). Horizontal axis is elapsed time since origin time (time=0 s) of each event. Onset time of S wave reported by the JMA is shown with arrows. (a) The possible LFE that occurred on February 26, 2003 (M 0.4). The epicentral distance is 27.6 km. (b) The possible LFE that occurred on January 31, 2004 (M 0.4). The epicentral distance is 33.4 km. (c) The possible LFE that occurred on July 18, 2005 (M 0.5). The epicentral distance is 27.2 km. (d) An LFE that occurred on April 21, 2006 (M 0.4). The epicentral distance is 30.8 km.
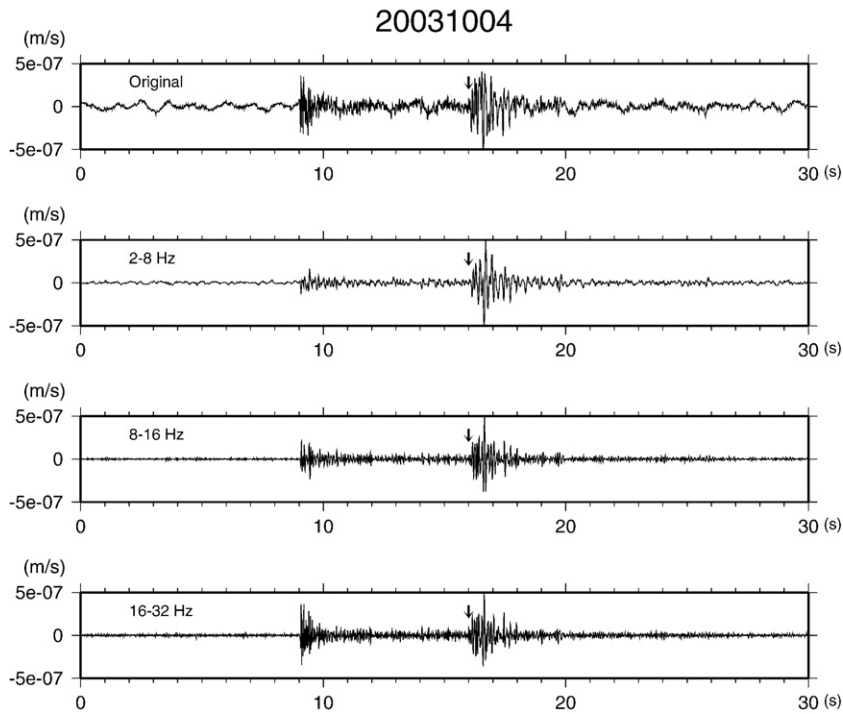
Fig. 3. The NS components of original and band-pass filtered (2–8, 8–16, 16–32 Hz) velocity seismic waveforms for a regular earthquake that occurred at a depth of about 50 km beneath eastern Kyushu on October 4, 2003 (M 0.8) recorded at a station with an epicentral distance of 28.4 km (from top to bottom). Horizontal axis is elapsed time since origin time (time = 0 s) of each event. Onset time of S wave reported by the JMA is shown with arrows.

occurred at depths of about 50 km beneath eastern Kyushu. Although there are high-frequency components, the amplitudes of 2–8 Hz are dominant relative to those of higher-frequency ranges, and the onset of the P wave is not clear. Similar results were found for the corresponding east–west (EW) components and NS components obtained at neighboring stations. These data are consistent with previous results showing that LFEs and LFTs in southwest Japan have amplitude spectrum peaks in the frequency range of 2 to 5 Hz (Kamaya and Katsumata, 2004). For comparison, we also assessed band-pass filtered seismic velocity waveforms recorded at a station with an epicentral distance of about 30 km for an LFE that occurred at a depth of about 30 km in western Shikoku (Fig. 2(d)). The characteristics of the filtered waveforms are almost identical to those shown in Fig. 2(a)–(c).

Fig. 3 shows an example of band-pass filtered seismic waveforms at a station with an epicentral distance of about 30 km for a regular micro-earthquake that occurred at a depth of about 50 km near the hypocenters of the two possible LFEs (February 26, 2003, and July 18, 2005, in Fig. 1 (b)) in eastern Kyushu. In contrast to the seismic waveforms of the three possible LFEs, the body waves at all frequency ranges had comparable amplitudes and we could clearly identify the onset of the P wave and the amplitude decay of the body waves. Therefore, our analyses strongly suggest that the three possible LFEs in eastern Kyushu were authentic LFEs.

2.3. Precise locations of the LFEs

Obtaining a precise location relative to regular intraslab micro-earthquakes is very important in quantitatively interpreting LFE occurrence. Therefore, we performed double-difference (DD) relocation analysis (Waldhauser and Ellsworth, 2000) to constrain the relative locations between the LFEs and regular intraslab earthquakes beneath Kyushu and the Kii Peninsula.

Although the original code of the hypoDD program adopts a 1-D velocity model to relocate earthquakes, that of DD tomography (tomoDD; Zhang and Thurber, 2003) uses a complex 3-D velocity model to relocate earthquakes. We used tomoFDD (Zhang and Thurber, 2006), which

employs a finite-difference travel-time algorithm and considers the curvature of the Earth, taking into account a recent 3-D velocity model (Hirose et al., 2007).

Hirose et al. (2007) divided southwest Japan into five sub-regions and estimated the 3-D seismic velocity structures by DD tomography for each region. Travel-time data recorded by the JMA from October 1, 1997 to December 31, 2005 were used. The distance between earthquake pairs was limited to 10 km in all regions. Grid intervals were set at 30–40 km along the direction of the Nankai Trough, 10–15 km perpendicular to the trough, and 5–10 km in the vertical direction. The initial velocity structure was taken from the JMA2001 velocity model (Ueno et al., 2002). A prominent feature revealed by Hirose et al. (2007) was a region with a low S-wave velocity (Vs) and high ratio of P-wave to S-wave velocities (Vp/Vs) of several kilometers in thickness immediately above the intraslab seismicity in a wide area from Tokai to Kyushu. This characteristic layer dipped shallowly in the direction of slab subduction. Compared to the upper surface of the PHS plate based on seismic re-fraction surveys of four survey lines, Hirose et al. (2007) interpreted these layers to correspond to the oceanic crust of the PHS slab. Based on the positions of these layers and the precisely relocated hypocenter distribution of intraslab earthquakes, they also delineated the upper surface of the PHS plate for the entire southwest Japan region.

We relocated the three LFEs beneath eastern Kyushu using the DD location technique (Waldhauser and Ellsworth, 2000). Arrival-time data of both regular earthquakes and LFEs were taken from the JMA catalogue, and differential travel times were constructed by directly subtracting travel times from event pairs within an inter-event distance of 10 km observed at common stations. Then, all the hypocenters including regular earthquakes were relocated using the 3-D velocity model by Hirose et al. (2007). In the relocation analysis, we used the initial locations of the three LFEs and regular earthquakes listed in the JMA database. Fig. 4(b) and (c) show the relocation results along with the upper plate surface of the PHS plate obtained by Nakajima and Hase-gawa (2007) and Hirose et al. (2007). All three events relocated around the upper surface of the PHS plate, suggesting that LFEs occur along the
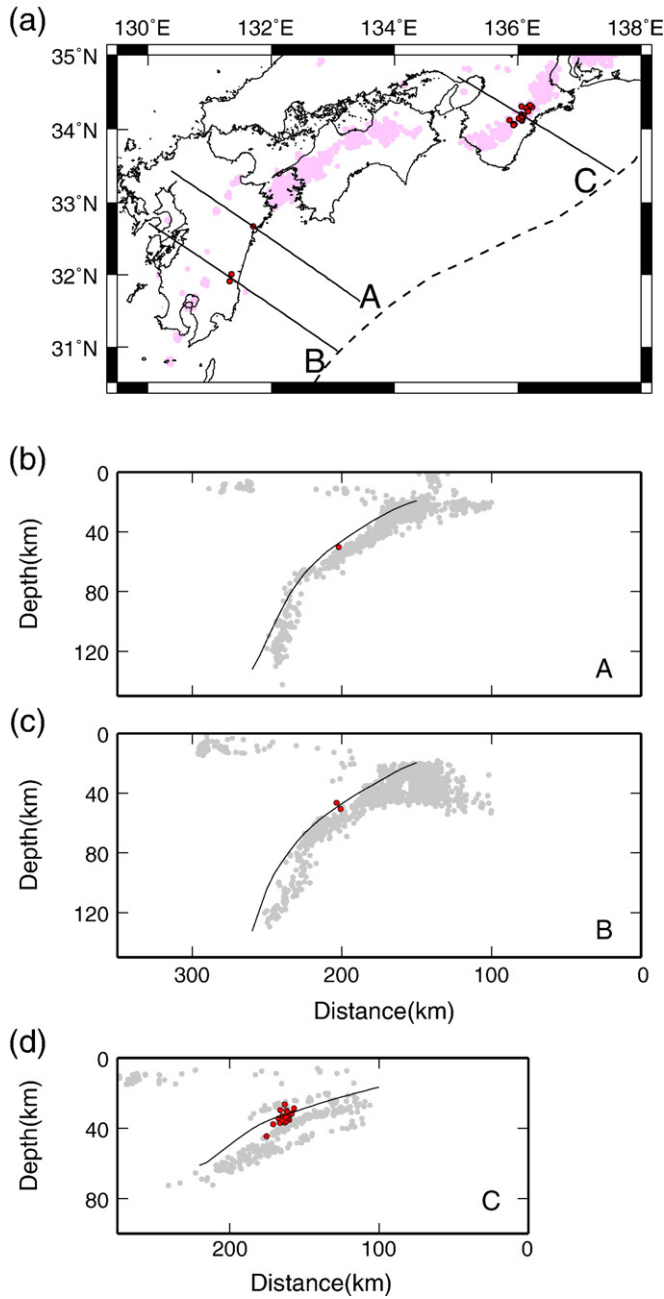
Fig. 4. (a) Map showing the location of the LFEs (red circles) that are relocated in this study with the 3-D velocity model (Hirose et al., 2007). Pink circles show other LFEs that are not relocated in this study. (b) Across-arc vertical cross section of the relocated LFE (red circle) together with regular intraslab earthquakes (gray circles) along profile A in (a). Earthquakes that occurred within 20 km from the profile are shown. (c) Across-arc vertical cross section of the relocated LFEs (red circles) together with regular intraslab earthquakes (gray circles) along profile B in (a). (d) Across-arc vertical cross section of the relocated LFEs (red circles) together with regular intraslab earthquakes (gray circles) along profile C in (a). Black curves in (b)–(d) denote the upper surface of the PHS plate estimated by Nakajima and Hasegawa (2007) and Hirose et al. (2007).

plate interface and/or within the oceanic crust beneath eastern Kyushu. Table 1 gives hypocenter information for the relocated LFEs.

Shelly et al. (2006) relocated microearthquakes, including LFEs, in western Shikoku using the DD tomography method (Zhang and Thurber, 2003). They showed that LFEs are located on the plate interface between the oceanic subducting PHS plate and the continental plate. The fault plane solutions of the LFEs indicate low-angle thrust faulting, suggesting LFE occurrence at the plate interface (Ide et al., 2007). The relocated depths were about 29–34 km (Shelly et al., 2006).

The JMA hypocenter catalogue includes many LFEs beneath the Kii Peninsula at depths of 30–50 km. To compare the depth ranges of LFEs to the temperature structures calculated in the following section, we selected 21 LFEs with more than 12 arrival-time data that took place within 20 km of the calculated temperature profile (line c in Fig. 5(a)). Using the DD method, we then relocated these LFEs together with the regular intraslab earthquakes that occurred around them. The 3-D model (Hirose et al., 2007) was used for relocation analysis, and the criteria for selecting event pairs were the same as those for eastern Kyushu. Fig. 4(d) shows the relocation results for the 21 LFEs. The relocated hypocenters are clustered at depths of 29–38 km, except for an LFE that occurred at a depth exceeding 40 km and appeared to be distributed above the NW-dipping intraslab earthquakes. The estimated upper surface of the PHS plate passes through the center of the LFE cluster. Although the scattered distribution of LFEs around the plate interface might add ambiguity to the interpretation of LFE occurrence, we conclude that LFEs took place around the plate interface beneath the Kii Peninsula as well as Kyushu and western Shikoku.

The relocated hypocenters suggest that LFEs occurred on the plate interface at depth ranges of approximately 50 km, 29–34 km, and 29–38 km beneath Kyushu, western Shikoku, and the Kii Peninsula, respectively. Although the estimated LFE depth beneath Kyushu was greater than the depths for the other two regions, the difference in the depth range between western Shikoku and the Kii Peninsula may not be significant because of errors in the estimation of absolute hypocenter locations and/or the scattered distribution of LFEs beneath the Kii Peninsula. In the following sections, we investigate the possibility that the dehydration reaction of oceanic basalt is related to LFE generation.

3. Method and model

To understand the dehydration process of oceanic basalt, which depends on pressure and temperature, it is necessary to have both the temperature structure associated with PHS plate subduction and a phase diagram for oceanic basalt. This section describes the model we used to calculate a temperature field.

Following Yoshioka and Sanshadokoro (2002), we calculated the temperature structure associated with slab subduction using numerical simulations for temperature and fluid flow in a 2-D box model. We assumed the continental crust to be a fixed conductive layer to a depth of 30 km. Thickness of the subducting slab d (km) is estimated as follows:

$$d = 7.5\sqrt{t}, \tag{1}$$

where t (Myr) is the age of the subducting plate (Yoshii, 1975) at the Nankai Trough. We set a uniform subducting velocity kinematically for the model domain corresponding to the slab. The momentum equation is as follows:

$$\frac{\partial^2}{\partial x \partial z}\left[4\eta \frac{\partial^2 \varphi}{\partial x \partial z}\right] + \left(\frac{\partial^2}{\partial z^2} - \frac{\partial^2}{\partial x^2}\right)\left[\eta\left(\frac{\partial^2}{\partial z^2} - \frac{\partial^2}{\partial x^2}\right)\varphi\right] = -\frac{\partial}{\partial x}(\rho_0 g \alpha T), \tag{2}$$

where x and z are the horizontal and vertical directions, respectively, φ is stream function, η is viscosity, ρ_0 is mantle density at room

Table 1
Relocated hypocenters for the three low-frequency earthquakes that occurred beneath eastern Kyushu

	Origin time	Magnitude	Latitude	Longitude	Depth (km)	Error in depth (km)
2003/2/26	03:48:41	0.4	31°55.61' N	131°17.42' E	50.5	1.1
2004/1/31	12:47:06	0.1	32°40.80' N	131°40.80' E	50.2	0.7
2005/7/18	01:46:57	0.5	31°59.17' N	131°18.20' E	46.3	1.0
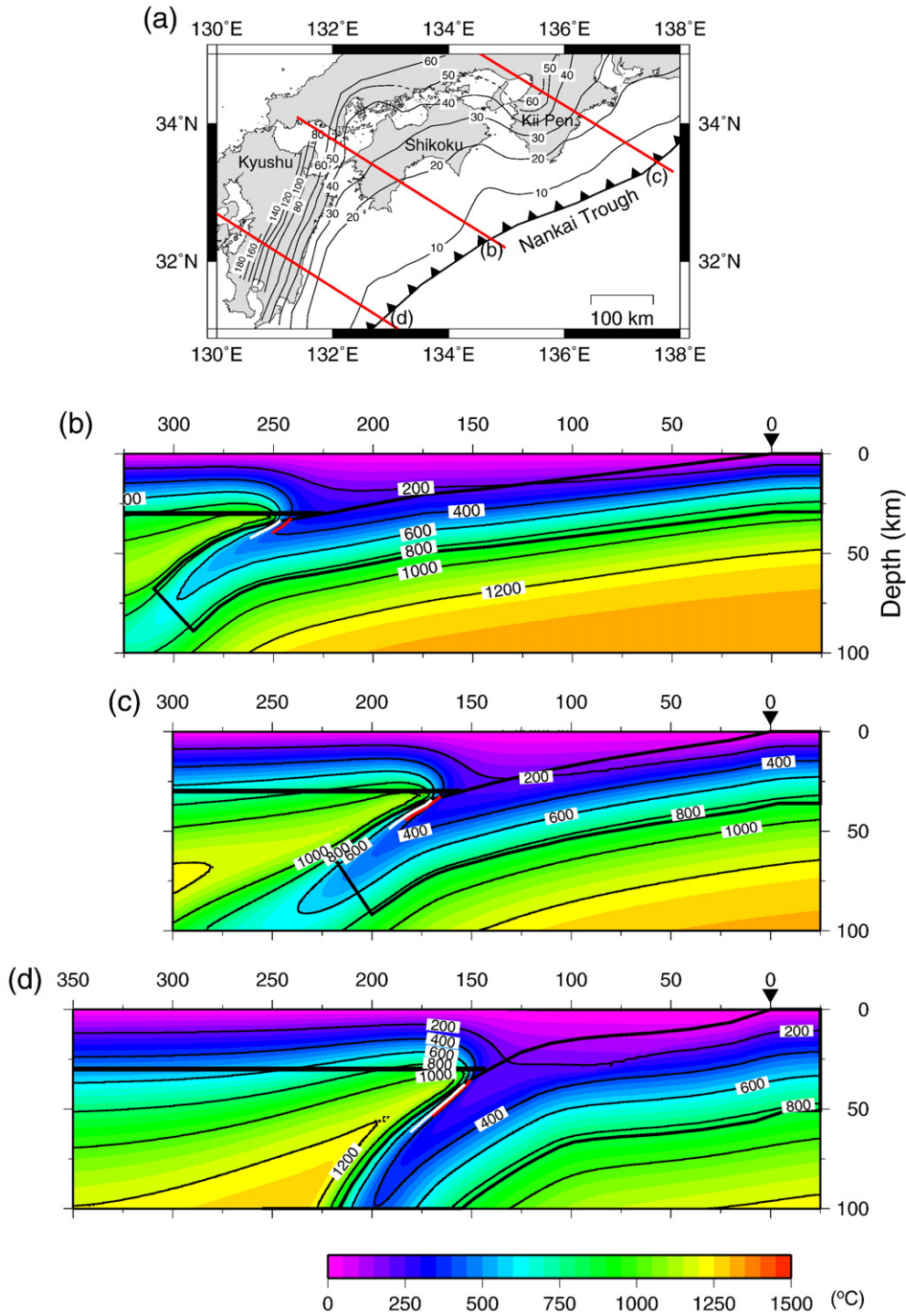
Fig. 5. (a) Map showing the locations of profiles (b), (c), and (d) along which temperature distributions associated with subduction of the PHS plate were calculated. (b) Temperature distribution along profile (b) shown in (a) passing through western Shikoku. The solid reverse triangle denotes the location of the Nankai Trough. The size of the model space is 500 km in horizontal distance and 300 km in depth, and a part of the whole modeling region is shown. The short red and white lines represent the locations where the first and second dehydration reactions, respectively, take place within the oceanic crust, which are calculated from the phase diagram of Fig. 6. (c) Temperature distribution along profile (c) shown in (a) passing through the Kii Peninsula. (d) Temperature distribution along profile (d) shown in (a) passing through eastern Kyushu.

temperature, g is gravity acceleration, α is thermal expansivity, and T is temperature. We assumed that mantle viscosity depended on temperature and depth and used Christensen's (1996) equation:

$$\eta = \eta_0 \exp\left(\frac{T_0 - T}{a} + \frac{z}{b} - \left(\frac{z}{c}\right)^2\right), \tag{3}$$

where η_0 is viscosity at temperature T_0 and depth $z=0$, and a, b, and c are constants. The energy equation is expressed as

$$\rho C_p \left(\frac{\partial T}{\partial t} + \boldsymbol{v} \cdot \nabla T\right) = k\nabla^2 T + v\rho_0 g\alpha T + 4\eta\left(\frac{\partial^2 \varphi}{\partial x \partial z}\right)^2 + \eta\left(\frac{\partial^2 \varphi}{\partial x^2} + \frac{\partial^2 \varphi}{\partial z^2}\right)^2, \tag{4}$$

Table 2
Model parameters used in temperature calculations

	Value	Unit
C_p	1.046[a]	kJ kg^{-1}
k	4.184[a]	Jm^{-1} K^{-1} s^{-1}
α	3×10^{-5}[b]	K^{-1}
T_0	1350[c]	°C
η_0	1×10^{20}[d]	Pa s
a	131.3[d]	K
b	236[d]	Km
c	1086[d]	Km
ρ_0	3400[e]	kg m^{-3}

[a] Hamaguchi et al. (1983).
[b] Iwamori (1997).
[c] Takenaka et al. (1999).
[d] Christensen (1996).
[e] Yoshioka and Sanshadokoro (2002).

where ρ is density, C_p is specific heat at constant pressure, t is time, $\boldsymbol{v}$ is the flow velocity vector, and k is thermal conductivity (Andrews, 1972). The second term on the left side is an advection term, and the first and second terms on the right side represent conduction and adiabatic compression, respectively. The third and fourth terms are viscous dissipation. The parameters used in the numerical simulation are given in Table 2.

Horizontally stratified temperature and no-flow conditions were considered initially. Then, we considered subduction of the oceanic PHS plate, the dipping length of which gradually increases with time, from the Nankai Trough along the present shape of the PHS plate in the convergence direction. The leading edge of the subducting oceanic plate is defined by the location showing the maximum depth of the upper surface of the PHS plate determined by the microearthquake distribution (Fig. 5(a)), although the slab that was calculated assuming an initiation of subduction at 15 Ma reached much more landward locations along each temperature profile (Fig. 5(b)–(d)).

Mantle flow was assumed to be associated with subduction of the PHS plate. The continental plate is composed of a rigid conductive layer, which was assigned a zero velocity, restricting it from participating in the viscous flow region. The rigid boundary condition was given at the interfaces between the continental crust and underlying mantle, and the mantle and subducting slab. For the three model boundaries except for the top boundary, material can flow freely in and out of the boundaries in the normal direction, with the exception of the domain occupying the oceanic plate which flows in from the right upper boundary.

For the initial layered temperature state, for simplicity, we used an equation for the cooling of an oceanic plate:

$$T = T_0 \mathrm{erf}\left(\frac{z}{2\sqrt{\frac{kt}{\rho C_p}}} \right), \qquad (5)$$

where erf is an error function and t is the age of the continental plate. The value of t is estimated from Eq. (1), assuming $d = 30$ km.

For the temperature boundary conditions, the model surface temperature was assumed to be 0 °C and a fixed temperature condition was given for the right boundary. The left and bottom boundaries were adiabatic.

Wang (2000) concluded that the Nankai subduction thrust fault is very weak, which is consistent with geothermal data. Therefore, we did not take into account any possible frictional heat acting on the plate interface in our model. We performed a numerical simulation of the temperature distribution and stream function in the model domain for western Shikoku, the Kii Peninsula, and eastern Kyushu by solving Eqs. (2) and (4) simultaneously, using a 2-D finite difference method.

4. Results and discussion

4.1. Temperature distribution profiles

Thermal structures associated with PHS plate subduction have been estimated in southwest Japan (e.g., Wang et al., 1995; Hyndman et al., 1995; Oleskevich et al., 1999; Peacock and Wang, 1999; Hacker et al., 2003b). Here we first discuss the differences between previous studies and the present study. To the best of our knowledge, all of those studies used source code developed by Wang et al. (1995) employing the finite element method (FEM) to calculate the thermal structures associated with slab subduction. In the source code, only the energy Eq. (4) in Section 3 is solved by giving flow velocity vectors that assume steady state flow patterns in the mantle wedge, which are obtained analytically. In contrast, we obtained both flow velocity vectors and temperature fields as a time-marching problem, by solving momentum (2) and energy (4) equations simultaneously as a coupled problem. Because the temperature field affects flow patterns, and vice versa, it is essential to solve the problem using the latter approach. In the studies by Wang et al. (1995), Hyndman et al. (1995), and Oleskevich et al. (1999), the former approach may have been permissible because they investigated the temperature field at the shallower plate interface, focusing on depths shallower than about 30 km in relation to the occurrence of megathrust earthquakes, where convection effects of the mantle wedge on the temperature field may be negligible because the oceanic and continental plates are treated as high viscous and conductive materials. On the other hand, Peacock and Wang (1999) and Hacker et al. (2003b) obtained a temperature field even at deeper depths, where the subducting oceanic plate contacts the overriding mantle wedge and convection effects cannot be ignored. In addition, although their models assumed a constant viscosity, it is well known that temperature and flow fields in the mantle wedge are different if temperature-dependent viscosity is adopted, which can affect the temperature field near the upper surface of the subducting oceanic plate. For these reasons, we believe that our model is more realistic.

In addition, the values of the subduction parameters (i.e., subduction velocity, direction of plate convergence, the age of the PHS plate, and the shape of its upper surface) used in previous studies were different from those used in this study, which were far more recent data. Thus, it is not possible to directly compare our results with those of previous studies.

We constructed models for profiles passing through western Shikoku, the Kii Peninsula, and eastern Kyushu (Fig. 5(a)), taking into account the complicated shape (Fig. 1(b)) of the subducting PHS plate estimated in recent studies (Baba et al., 2002; Hirose et al., 2007; Nakajima and Hasegawa, 2007). The size of the model space was set to 500 km in horizontal distance and 300 km in depth for the three profiles. We used a convergence rate and direction of the subducting PHS plate estimated from Global Positioning System (GPS) data (Sella et al., 2002) (Fig. 1(b)).

The Shikoku Basin (PHS plate) initiated subduction beneath the continental plate northwestward along the Nankai Trough at 15 Ma (e.g., Underwood et al., 1993). Thus, we calculated the temperature field associated with PHS plate subduction at present (0 Ma), giving the initial and boundary conditions for temperature and fluid flow at 15 Ma. In addition, we considered the age difference of the PHS plate along the margin-parallel direction. According to a magnetic anomaly study (Okino et al., 1994), the age of the Kinan Seamount Chain, which is the youngest underlying the northern part of the PHS plate, is 15 Ma, and the age gradually increases in the east–northeast and west–southwest directions. Thus, we assumed that the ages of the PHS plate at the Nankai Trough for western Shikoku and the Kii Peninsula were 15 and 23 Ma, respectively, taking into account the spreading rate of the Shikoku Basin before 15 Ma.

Tokuyama (1995) demonstrated that the ages of the Amami Plateau and the Daito Ridge, which are located far south of Kyushu, are 82–85

and 57–82 Ma, respectively (Fig. 1(a)). Although the age of the Kyushu–Palau Ridge has not been estimated from magnetic anomalies, Yoshioka (2007) estimated its age at approximately 46 Ma based on a comparison between observed low heat flow data off southeastern Kyushu and calculations using 3-D subduction models. Therefore, we calculated the temperature structure along eastern Kyushu using an age of 46 Ma for the subducting PHS plate at the Nankai Trough.

Fig. 5(b)–(d) show the calculated temperature distributions along the profiles passing through western Shikoku, the Kii Peninsula, and eastern Kyushu, respectively. The subducting PHS plate beneath western Shikoku and the Kii Peninsula is younger and hotter than that beneath eastern Kyushu. The results show that temperatures 15 km inside from the upper surface of the PHS plate at a depth of 50 km are approximately 500 °C and 400 °C beneath western Shikoku and the Kii Peninsula, respectively. Because the isotherms near the upper surface of the PHS plate beneath western Shikoku and the Kii Peninsula cross the plate interface at a slanted orientation, temperature increases dramatically in the down–dip direction (Figs. 5(b), (c), 6(a), and (b)).

On the other hand, the temperature at the corresponding location beneath eastern Kyushu is approximately 300 °C, and low temperature is preserved at greater depths. The slabs beneath western Shikoku and the Kii Peninsula have linear shapes with low dip angles, whereas the slab beneath eastern Kyushu is bent with a high dip angle. Thus, hot mantle material flows into the shallow part of the mantle wedge, and the surface of the slab is heated rapidly, resulting in the large temperature gradient toward the inside of the slab. Because the isotherms near the upper surface of the PHS plate beneath eastern Kyushu are almost parallel to the down–dip direction, the temperature does not change much in that direction (Figs. 5(d) and 6(c)). The temperatures at the locations of LFEs were estimated at approximately 400–500 °C in southwest Japan; this temperature range is consistent with results obtained using the 3-D subduction model (Yoshioka and Murakami, 2007).

4.2. Regionality of LFEs from the phase diagram of basalt+H₂O

Shelly et al. (2006) identified a region with a high Vp/Vs ratio between LFEs and intraslab microearthquakes in western Shikoku, indicating the existence of fluid in the oceanic sedimentary layer and/or oceanic crust just below the LFEs. Hydrous minerals such as clay, zeolite, chlorite, and mica are included in the oceanic sedimentary layer and may exist even at high pressures and temperatures. Thus, it is possible for muddy sedimentary rock to transport water to depths of the mantle transition zone (Ono, 2000). Therefore, it is unlikely that dehydration from the oceanic sedimentary layer at a specific pressure and temperature at depths of around 30 km generates LFEs (Kamaya and Katsumata, 2004). For this reason, we tested the idea that dehydration of hydrous minerals of oceanic basalt at a certain pressure and temperature of subducting oceanic crust may cause LFEs (Katsumata and Kamaya, 2003).

We used the phase diagram of Hacker et al. (2003a) for water-saturated basalt. The temperature and pressure of an oceanic plate increase with subduction, resulting in phase transformations of hydrous minerals in the subducting oceanic crust. Water content varies, depending on the composition of hydrous minerals, and different dehydration reactions take place at different pressures and temperatures. Two remarkable dehydration reactions occur on the green equilibrium lines shown in Fig. 6(a): one related to phase transformations from domains A and B to C, D, and E, and the other from domains C, D, and E to F and G. Most are related to phase transformations of lawsonite+blueschist+jadeite to amphibole+eclogite. The associated decreases in water content are approximately 2.4 wt.%.

Peacock and Wang (1999), Hacker et al. (2003b), and Katsumata and Kamaya (2003) used similar approaches and demonstrated possible temperature and pressure ranges associated with PHS plate subduction on the phase diagram for mid-ocean-ridge basalt (MORB). However, a direct comparison with our results is impossible because of the reasons described in Section 4.1.

Fig. 6(a)–(c) show temperature–depth paths along depths of 0–5 km below the upper surface. These paths correspond to a domain occupying the oceanic crust of the PHS plate along the profiles passing through western Shikoku, the Kii Peninsula, and eastern Kyushu, respectively (Fig. 5(a)). Below western Shikoku, the temperature and depth ranges were approximately 380–410 °C and 34–40 km for the first reaction and approximately 500–520 °C and 34–42 km for the second one (Fig. 6(a)). On the other hand, the depths of the LFE hypocenters in western Shikoku ranged from approximately 29 to 34 km (Shelly et al., 2006). Thus, taking into account the 5-km-thick oceanic crust and local dip angle, LFEs
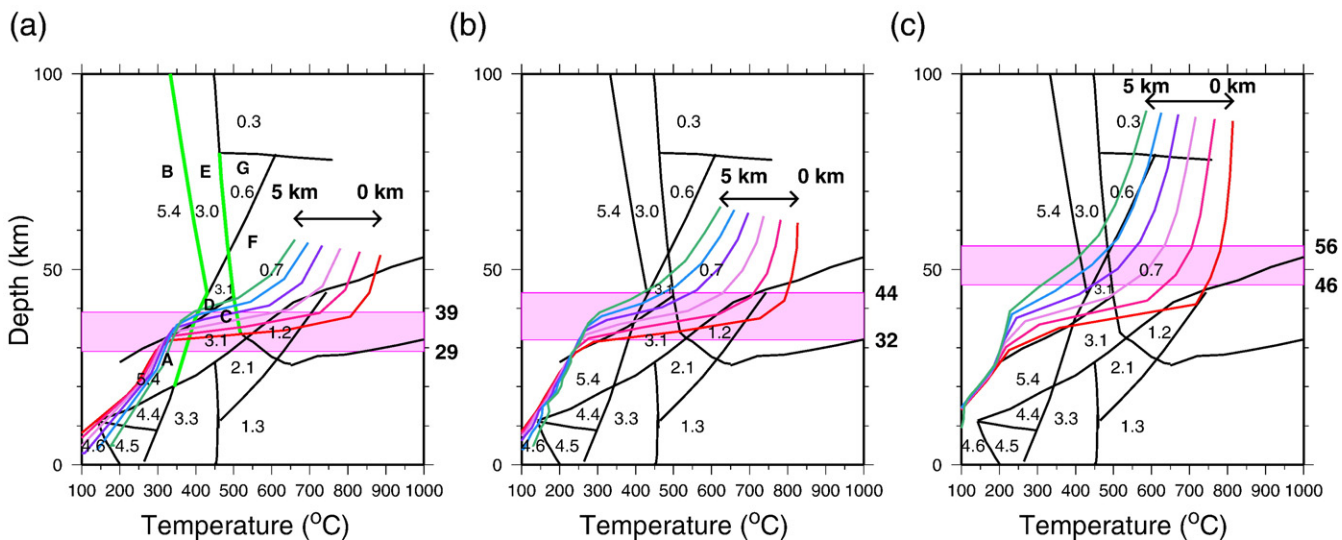

Fig. 6. Calculated temperature-depth paths along the upper surface of the subducting PHS plate, which are plotted on a phase diagram of basalt+H₂O (Hacker et al., 2003a). The six curved lines are temperature–depth paths at depths of 0 to 5 km below the upper surface of the PHS plate. Dehydration reaction takes place on the green and black lines. The water content (wt%) for each domain is shown in numeral. A possible water-supplied depth range to generate LFEs is shown in the pink belt. The depth ranges were estimated from relocated hypocenter depths of LFEs by Shelly et al. (2006) and those obtained in this study. (a) western Shikoku. The alphabets A to G indicate different domains in the phase diagram. The green lines denote remarkable dehydration for the subducting PHS plate. (b) the Kii Peninsula. (c) eastern Kyushu.

generated by water dehydration would originate in the crust at 29–39 km depth, assuming that water included in the crust just below the LFEs is involved in the LFE generation. This is consistent with the depth ranges of the two dehydration reactions.

Below the Kii Peninsula, the temperature and depth ranges were approximately 385–430 °C and 32–45 km for the first reaction and approximately 490–520 °C and 34–49 km for the second one (Fig. 6(b)), respectively. The relocated hypocenter depths of LFEs beneath the Kii Peninsula were approximately 29–38 km (Fig. 4(d)), resulting in 32–44 km as the water-supplied depth range of the oceanic basalt located just below the LFEs. This is similar to the depth ranges of the two dehydration reactions.

The water-supplied depth range related to LFEs was 29–39 km for western Shikoku and 32–44 km for the Kii Peninsula. Although the difference in depth ranges cannot be discussed because of errors in estimating the absolute hypocenter locations and/or the scattered distribution of LFEs, the depth ranges of the dehydration reactions estimated from the calculated temperature–depth paths and the phase diagram for the Kii Peninsula were deeper and broader than the depth range estimated for western Shikoku. This difference in the ranges was discernible even if model and parameter uncertainties were considered because the dip angle and the age of the slab below the Kii Peninsula are larger than those below western Shikoku. Therefore, hotter mantle material flows into the seaward corner of the mantle wedge below the Kii Peninsula (Yoshioka and Murakami, 2007), resulting in a smaller temperature change in the slab in the dipping direction (Figs. 5(b), (c), 6(a), and (b)).

On the other hand, because of a large temperature gradient toward the inside of the slab, the possible depth range of the dehydration reaction estimated from the width of the six temperature–depth paths for eastern Kyushu was broader than that for western Shikoku and the Kii Peninsula (Fig. 6(a)–(c)). The expected temperature and depth ranges of the dehydration reactions beneath eastern Kyushu were approximately 390–430 °C and 36–53 km for the first reaction and approximately 480–520 °C and 38–62 km for the second one. The relocated hypocenter depths of the three LFEs were 46–51 km (Table 1), and thus the depth range of dehydration based on those hypocenter depths was 46–56 km. From Fig. 6(c), it might be possible to correlate LFE occurrence with the dehydration reactions of hydrous minerals of the oceanic basalt beneath eastern Kyushu. However, unlike Shikoku and the Kii Peninsula, the belt-like occurrence of LFEs was not identified in eastern Kyushu.

Based on these findings, we considered the possible reasons for the rarity of LFEs beneath eastern Kyushu compared to western Shikoku and the Kii Peninsula. Severe dehydration is expected when the six depth–temperature paths on the phase diagram in Fig. 6 cross the two equilibrium lines shown in green in Fig. 6(a). The associated decrease in water amount is approximately 2.4 wt.% irrespective of depth and temperature on the two equilibrium lines. To investigate the regional differences in dehydrated water, we plotted the two equilibrium lines in the oceanic crust on the calculated temperature fields in Fig. 5(b)–(d). We defined dehydrated water per unit length, assuming that the incoming hydrous minerals consisting of subducted oceanic crust were diluted during the phase transformations along the two delineated lines. The dehydrated water per unit length for western Shikoku, the Kii Peninsula, and eastern Kyushu was 0.19, 0.12, and 0.08 wt.%/km, respectively. If all three regions were assumed to have the same hydrous minerals in the subducted oceanic crust, this result indicated that eastern Kyushu had the lowest value of dehydrated water per unit length. In addition, unlike western Shikoku and the Kii Peninsula, the Kyushu–Palau Ridge, which is mainly composed of tonalite and lacks hydrous minerals, is subducting beneath eastern Kyushu (Seno and Yamasaki, 2003). Therefore, a remarkable steady dehydration reaction does not take place, but a dehydration reaction for a small amount of hydrous minerals may occur at a specific pressure–temperature condition, generating LFEs beneath eastern

Kyushu at approximately 50 km depth. This would help explanation of the rarity of LFEs beneath eastern Kyushu.

Hasegawa et al. (2007) noted that the inherent nature of a plate boundary is another important factor that could trigger LFEs. LFEs and LFTs occur in the transition zone from locked to aseismic slip zones on the plate boundary (Obara and Hirose, 2006). The depth ranges of dehydration reactions 29–44 km beneath western Shikoku and the Kii Peninsula correspond to the transition zone on the plate boundary, whereas the depth ranges of the dehydration reactions in eastern Kyushu, which are estimated at 44–56 km, may correspond to the aseismic slip zone. This difference could also result in the regionality of LFEs.

In this study we suggested possible explanations for the rarity of LFEs beneath eastern Kyushu. This kind of study may be helpful to understand that absence of LFEs and LFTs in other regions such as northeast Japan, the Kanto district, and Kii channel is either due to low detectability of the seismic network or real absence of these events.

5. Conclusions

We quantitatively investigated three possible LFEs recently recorded beneath eastern Kyushu (Fukuoka District Meteorological Observatory, 2004a) and examined the regionality of LFE occurrence in western Shikoku, the Kii Peninsula, and eastern Kyushu based on temperature calculations for 2-D subduction models of slabs with arbitrary shapes. Our study produced the following significant results:

(1) The three recordings below eastern Kyushu were very likely authentic LFEs.
(2) All three LFEs were relocated near the upper surface of the subducting PHS plate at depths of approximately 50 km.
(3) The hypocenters of relocated LFEs below the Kii Peninsula ranged from depths of 29–38 km. These LFEs appear to be distributed above NW-dipping intraslab regular microearthquakes. The upper interface of the PHS plate passes through the cluster of relocated LFEs.
(4) The estimated depth ranges of the dehydration reactions associated with PHS plate subduction from the temperature–depth paths on the phase diagram agreed well with water-supplied depth ranges estimated from LFE hypocenters beneath western Shikoku and the Kii Peninsula, indicating that LFE generation is closely related to steady-state dehydration processes. The corresponding temperature range was approximately 400–500 °C.
(5) The temperature gradient toward the inside of the subducting PHS slab below eastern Kyushu was larger than that below western Shikoku and the Kii Peninsula. This is because hot mantle material flows into the seaward corner of the mantle wedge below eastern Kyushu due to the high dip angle there. As a result, temperature–depth paths for the oceanic crust along the dipping direction below eastern Kyushu have more diversity than those below western Shikoku and the Kii Peninsula on the phase diagram.
(6) Using the calculated thermal structures and phase diagram of water dehydration for oceanic basalt, the amount of water dehydration per unit length, which was newly defined in this study, was estimated as 0.19, 0.12, and 0.08 wt.%/km for western Shikoku, the Kii Peninsula, and eastern Kyushu, respectively; that is, the region beneath eastern Kyushu has the lowest water dehydration rate value. Considering that the Kyushu–Palau Ridge that is subducting beneath eastern Kyushu is composed of tonalite, which is low in hydrous minerals, this finding suggests that the regional differences in the occurrence frequency of LFEs may be related to the amount of water dehydration associated with subduction of the PHS plate and/or differences in LFE depths. This indicates that a steady dehydration reaction associated with plate subduction does not take place beneath eastern Kyushu, but a dehydration reaction

may occur at a specific pressure–temperature condition, generating LFEs beneath eastern Kyushu at depths of approximately 50 km.

Acknowledgments

References

Ando, M., 1975. Source mechanisms and tectonic significance of historical earthquakes along the Nankai Trough. Tectonophysics 27, 119–140.

Andrews, D.J., 1972. Numerical simulation of sea-floor spreading. J. Geophys. Res. 77, 6470–6481.

Baba, T., Tanioka, Y., Cummins, P.R., Uhira, K., 2002. The slip distribution of the 1946 Nankai earthquake estimated from tsunami inversion using a new plate model. Phys. Earth Planet. Inter. 132, 59–73.

Christensen, U.R., 1996. The influence of trench migration on slab penetration into the lower mantle. Earth Planet. Sci. Lett. 14, 27–39.

Fukuoka District Meteorological Observatory, 2004a. Seismic activity in and around Kyushu and Yamaguchi Prefecture in February, 2004, pp. 1–17 (in Japanese).

Fukuoka District Meteorological Observatory, 2004b. Seismic activity in and around Kyushu and Yamaguchi Prefecture in November, 2004, pp. 1–22 (in Japanese).

Hacker, B.R., Abers, G.A., Peacock, S.M., 2003a. Subduction Factory 1. Theoretical mineralogy, densities, seismic wave speeds, and H_2O contents. J. Geophys. Res. 108. doi:10.1029/2001JB001127.

Hacker, B.R., Abers, G.A., Peacock, S.M., 2003b. Subduction Factory 2. Are intermediate–depth earthquakes in subducting slabs linked to metamorphic dehydration reactions? J. Geophys. Res. 108. doi:10.1029/2001JB001129.

Hamaguchi, H., Goto, K., Suzuki, Z., 1983. Double-planed structure of intermediate–depth seismic zone and thermal stress in the descending plate. J. Phys. Earth 31, 329–347.

Hasegawa, A., Nakajima, J., Hirose, F., 2007. Phase transformation depth in the slab crust and upper-plane seismic belts as its manifestation — does it control the generation of short-term slow slip events and deep seismic tremors? Monthly Earth 29, 364–375 (in Japanese).

Hirose, F., Nakajima, J., Hasegawa, A., 2007. Three-dimensional velocity structure in southwestern Japan and configuration of the Philippine Sea slab estimated by double-difference tomography. J. Seis. Soc. Jpn. 60, 1–20 (in Japanese with English abstract).

Hyndman, R.D., Wang, K., Yamano, M., 1995. Thermal constraints on the seismogenic portion of the southwestern Japan subduction thrust. J. Geophys. Res. 100, 15373–15392.

Ide, S., Shelly, D.R., Beroza, G.C., 2007. The mechanism of deep low frequency earthquakes: Further evidence that deep non-volcanic tremor is generated by shear slip on the plate interface. Geophys. Res. Lett. 34, L03308. doi:10.1029/2006GL028890.

Ito, Y., Obara, K., 2006. Dynamic deformation of the accretionary prism excites very low-frequency earthquakes. Geophys. Res. Lett. 33, L02311. doi:10.1029/2005GL025270.

Iwamori, H., 1997. Heat sources and melting in subduction zones. J. Geophys. Res. 102, 14803–14820.

Kamaya, N., Katsumata, A., 2004. Low-frequency events away from volcanoes in the Japan Islands. J. Seis. Soc. Jpn. 57, 11–28 (in Japanese with English abstract).

Katsumata, A., Kamaya, N., 2003. Low-frequency continuous tremor around the Moho discontinuity away from volcanoes in the southwest Japan. Geophys. Res. Lett. 30, 1020. doi:10.1029/2002GL015981.

Nakajima, J., Hasegawa, A., 2007. Subduction of the Philippine Sea slab beneath southwestern Japan: slab geometry and its relationship to arc magmatism. J. Geophys. Res. 112, B08306. doi:10.1029/2006JB004770.

Obara, K., 2002. Nonvolcanic deep tremor associated with subduction in southwest Japan. Science 296, 1679–1681.

Obara, K., Hirose, H., 2006. Non-volcanic deep low-frequency tremors accompanying slow slips in the southwest Japan subduction zone. Tectonophysics 417, 33–51.

Okino, K., Shimakawa, Y., Nagaoka, S., 1994. Evolution of the Shikoku Basin. J. Geomagn. Geoelectr. 46, 463–479.

Oleskevich, D.A., Hyndman, R.D., Wang, K., 1999. The updip and downdip limits to great subduction earthquakes: Thermal and structural models of Cascadia, south Alaska, SW Japan, and Chile. J. Geophys. Res. 104, 14965–14991.

Ono, S., 2000. Hydrous minerals and water transport in subducted slab. J. Geogr. 109, 564–575 (in Japanese).

Peacock, S.M., Wang, K., 1999. Seismic consequences of warm versus cool subduction metamorphism: Examples from southwest and northeast Japan. Science 286, 937–939.

Sella, G.F., Dioxin, T.H., Mao, A., 2002. REVEL: a model for Recent plate velocities from space geodesy. J. Geophys. Res. 107, B4. doi:10.1029/2000JB000033.

Seno, T., Yamasaki, T., 2003. Low-frequency tremors, intraslab and intraplate earthquakes in Southwest Japan from a viewpoint of slab dehydration. Geophys. Res. Lett. 30, 2171. doi:10.1029/2003GL018349.

Shelly, D.R., Beroza, G.C., Ide, S., Nakamura, S., 2006. Low-frequency earthquakes in Shikoku, Japan, and their relationship to episodic tremor and slip. Nature 442, 188–191.

Takenaka, S., Sanshadokoro, H., Yoshioka, S., 1999. Velocity anomalies and spatial distributions of physical properties in horizontally lying slabs beneath the Northwestern Pacific region. Phys. Earth Planet. Inter. 112, 137–157.

Tokuyama, H., 1995. Origin and Development of the Philippine Sea. Geol. Geophys. Philipp. Sea 155–163.

Ueno, H., Hatakeyama, S., Aketagawa, T., Funasaki, J., Hamada, N., 2002. Improvement of hypocenter determination procedures in the Japan Meteorological Agency. Q. J. Seism. 65, 123–134 (in Japanese with English abstract).

Underwood, M.B., Bryne, T., Hibbard, J.P., DiTullio, L., Laughland, M.M., 1993. The effects of ridge subduction on the thermal structure of accretionary prisms: a Tertiary example from the Shimanto Belt of Japan. In: Underwood, M.B. (Ed.), Thermal evolution of the Tertiary Shimanto belt, southwest Japan: An example of ridge–trench interaction. Geol. Soc. Am. Spec. Pap., vol. 273, pp. 151–168.

Waldhauser, F., Ellsworth, W.L., 2000. A double-difference earthquake location algorithm: method and application to the northern Hayward Fault, California. Bull. Seismol. Soc. Am. 90, 1353–1368.

Wang, K., 2000. Stress–strain, 'paradox', plate coupling, and forearc seismicity at the Cascadia and Nankai subduction zones. Tectonophysics 319, 321–338.

Wang, K., Hyndman, R.D., Yamano, M., 1995. Thermal regime of the Southwest Japan subduction zone: effects of age history of the subducting plate. Tectonophysics 248, 53–69.

Wei, D., Seno, T., 1998. Determination of the Amurian plate motion, in mantle dynamics and plate interactions in East Asia. Geodynamics Series 27. American Geophysical Union, Washington, D.C., pp. 337–346.

Wessel, P., Smith, W.H.F., 1998. New improved version of the Generic Mapping Tools released. EOS Trans. AGU 79, 579.

Yoshii, T., 1975. Regionality of group velocities of Rayleigh waves in the Pacific and thickening of the plate. Earth Planet. Sci. Lett., 25, 305–312.

Yoshioka, S., 2007. Difference in the maximum magnitude of interplate earthquakes off Shikoku and in the Hyuganada region, southwest Japan, inferred from the temperature distribution obtained from numerical modeling — the proposed Hyuganada triangle. Earth Planet. Sci. Lett. 263, 309–322.

Yoshioka, S., Murakami, K., 2007. Temperature distribution of the upper surface of the subducted Philippine Sea Plate along the Nankai Trough, southwest Japan, from a three-dimensional subduction model: relation to large interplate and low-frequency earthquakes. Geophys. J. Int. 171, 302–315.

Yoshioka, S., Sanshadokoro, H., 2002. Numerical simulations of deformation and dynamics of horizontally lying slabs. Geophys. J. Int. 151, 69–82.

Zhang, H., Thurber, C.H., 2003. Double-difference tomography: the method and its application to the Hayward Fault, California. Bull. Seismol. Soc. Am. 93, 1875–1889.

Zhang, H., Thurber, C.H., 2006. Development and applications of double-difference seismic tomography. Pure Appl. Geophys. 163, 373–403.